SCIENCE CHINA
Chemistry

• REVIEWS •
· SPECIAL TOPIC · Electrochemical Power Sources

December 2017 Vol.60 No.12: 1494–1507
doi: 10.1007/s11426-017-9153-6

Noble metal-free catalysts for oxygen reduction reaction

Xiaoxiao Huang, Yazhou Wang, Wei Li & Yanglong Hou*

Beijing Key Laboratory for Magnetoelectric Materials and Devices, Beijing Innovation Center for Engineering Science and Advanced Technology, Department of Materials Science and Engineering, College of Engineering, Peking University, Beijing 100871, China

Received July 10, 2017; accepted October 12, 2017; published online November 17, 2017

Developing noble metal-free catalysts with low cost, high performance and stability for oxygen reduction reaction (ORR) in fuel cells is of great interest to promote sustainable energy devices. In this review, we summarized noble metal-free catalysts for ORR, including non-noble metal-based and heteroatom-doped carbon nanomaterials. Mesoporous structure, homogeneous distribution of nanocrystals and synergistic effect of carbon base and nanocrystals/doped heteroatoms have great effect on the ORR property. The noble metal-free nanomaterials showed comparable catalytic property, better stability and methanol tolerance than commercial platinum (Pt)-based catalysts, showing great potential as substitutes for noble metal-based catalysts. In addition, the challenges and chances of developing noble metal-free ORR catalysts are also discussed.

ORR, noble metal-free catalyst, stability, methanol tolerance

Citation: Huang XX, Wang YZ, Li W, Hou YL. Noble metal-free catalysts for oxygen reduction reaction. *Sci China Chem*, 2017, 60: 1494–1507, doi: 10.1007/s11426-017-9153-6

1 Introduction

In recent decades, rapid development of industry and increasing environment pollution are calling for more environmental friendly and highly efficient energy devices, especially the one powered by renewable energy resources. Fuel cell is known as one new device of energy conversion with the advantages of high efficiency, high reliability and so on [1,2]. Whereas, high-cost and low-stability catalysts for oxygen reduction reaction (ORR) as well as the production and storage of H_2 are two main obstacles for the promotion of fuel cells [3,4].

In a typical H_2-O_2 fuel cell, the fuel is oxidized at the anode, which provides the electron for the reduction reaction at the cathode. Accordingly, oxygen is reduced into water molecules or hydroxyl ions at the cathode. The half reactions in acid electrolyte can be shown below, including hydrogen oxidation reaction (HOR) at anode and ORR at cathode compared to the reversible hydrogen electrode (RHE):

$$\text{HOR:}\quad 2H_2 \rightarrow 4H^+ + 4e^-,\quad E^0 = 0\ \text{V (vs. RHE)} \tag{1}$$

$$\text{ORR:}\quad O_2 + 4H^+ + 4e^- \rightarrow 2H_2O,\quad E^0 = 1.23\ \text{V (vs. RHE)} \tag{2}$$

In fuel cells, the reaction of oxygen reduction at the cathode is sluggish. Theoretically, the dynamic efficiency of H_2-O_2 fuel cells can reach over 80% at room temperature, but the practical efficiency is only about 10%–20%, which is mainly due to the ORR at the cathode [5]. In order to improve the efficiency of fuel cells, catalysts for ORR are in great needed. Noble metal Pt has been confirmed the most efficient catalyst for ORR [6]. However, the commercially 20 wt% Pt nanoparticles (NPs) loaded on the Ketjen carbon (20% Pt/C) suffers from high cost, low stability, and poor tolerance of methanol [7]. As a result, exploration for highly efficient, low-cost and more stable catalysts for ORR is a key issue for the promotion of fuel cells.

*Corresponding author (email: hou@pku.edu.cn)

There are great efforts on exploring efficient ORR catalysts over the past decades, which have provided more possibility for the promotion of fuel cells. The following ideas have been put forward to deal with the problems.

Firstly, alloying the Pt NPs or structuring various shapes of Pt nanocrystals with plenty of exposed active crystal faces, which can lower the cost of the catalysts with comparable or even higher catalytic property than 20% Pt/C [8–16].

Secondly, developing the non-noble metal-based catalysts, which are mainly based on iron (Fe), cobalt (Co), and nickel (Ni) and so on [17–24].

Thirdly, designing metal-free catalysts, such as nitrogen (N), phosphorus (P)-doped carbon nanocatalysts [25–27].

There have been lots of reviews on the Pt-based catalysts, in which the surface electronic effects and structures are fully discussed in improving the catalytic performance [28–30]. Nowadays, significant advances in exploration of nanochemistry and nanomaterials have stimulated the researches in developing nanomaterials on ORR catalysts. Nanomaterials without noble metals have shown comparable ORR activity to Pt, but superior methanol tolerance and stability. More and more interesting researches have been directed to design noble metal-free catalysts. In this review, we will mainly focus on recent development about the ORR catalysts based on non-noble metal and non-metal nanomaterials. At first, we will present the mechanism of ORR, regular test methods and parameters for better understanding of the following discussion. Then we will discuss the non-noble metal-based catalysts, including metal oxide, metal carbide, and metal nitride, among which the non-noble metal-nitrogen/carbon (M–N/C) active sites will be highlighted. The influence of morphology of catalysts, coordination between NPs and substrate along with the structure of NPs on catalysts will be discussed. In addition, synthesis and ORR performance of heteroatom-doped carbon nanomaterials (N, P and so on) were illustrated. Furthermore, we will conclude the challenges and chances of designing noble metal-free catalysts.

2 Mechanism and testing method

2.1 Reaction pathways of ORR

The ORR reaction takes place by two pathways: 2-electron pathway and 4-electron pathway [31]. Both of the pathways are shown in Figure 1. The 2-electron pathway of ORR, which is also called partial reduction, involves an intermediate product-adsorbed hydrogen peroxide. Whereas, the 4-electron pathway (full reduction) does not involve the production of hydrogen peroxide, which is believed a better choice for its improved efficiency and high reactivity of hydrogen peroxide compared to the stability of water. In the 2-electron pathway, oxygen molecule is firstly adsorbed on the catalyst surface to form an adsorbed oxygen molecule (marked as $*O_2$). The $*O_2$ can absorb electron and react with the hydrogen ions to form the absorbed hydrogen peroxide, which will undergo further reduction to generate two water molecules or simple dissociation to produce a hydroxide molecule. In the 4-electron process, *OOH is produced, following the O_2 adsorption. The 4-electron pathway is divided into two mechanisms by the place where the second hydrogen addition takes place. If the second hydrogen addition takes place at the oxygen adsorbed to the catalyst (mechanism 1), two adsorbed *OH groups will be produced. Later, hydrogen addition and electron transfer take place at each *OH group, producing two water molecules. On the other situation, the second hydrogen addition takes place at the oxygen already bound to hydrogen (mechanism 2), resulting in desorption of a H_2O and adsorption of O atom. The second water molecule is formed by hydrogen addition to the *O. Mechanism 1 has been proved more thermodynamically favored by density functional theory (DFT) simulations [3,32,33].

Mechanism 1:

$$\begin{aligned} &O_2 \rightarrow *O_2 \\ &*O_2 + e^- + H^+ \rightarrow *OOH \\ &*OOH + e^- + H^+ \rightarrow *OH + *OH \\ &2*OH + 2e^- + 2H^+ \rightarrow 2H_2O \end{aligned} \tag{3}$$

Mechanism 2:

$$\begin{aligned} &O_2 \rightarrow *O_2 \\ &*O_2 + e^- + H^+ \rightarrow *OOH \\ &*OOH + e^- + H^+ \rightarrow *O + H_2O \\ &*O + e^- + H^+ \rightarrow *OH \\ &*OH + e^- + H^+ \rightarrow H_2O \end{aligned} \tag{4}$$

2.2 Regular measurements of ORR catalysts

There are several methods for regular measurements of ORR catalysts, with relative strengths and weaknesses. For example, the gas diffusion electrodes method/fuel cell membrane electrode assemblies with a typical two-electrode setup can demonstrate the function of catalysts in practical devices [6,34]. Whereas, this measurement demands thick layers composed of carbon, binder in addition to the catalysts, which may be difficult to measure the specific activity due to the ill-defined catalyst active sites and sluggish mass transport.

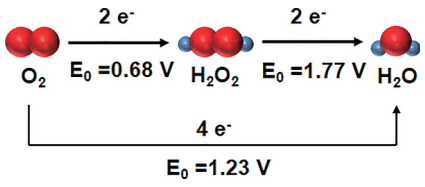

Figure 1 Scheme of the ORR mechanism by direct pathway and indirect pathway (color online).

Commonly, the rotating disk electrode (RDE)/rotating ring-disk electrode (RRDE) measurements can overcome the drawbacks of oxygen transport [35]. Thin film can be produced in RDE/RRDE measurements due to the dispersed ink of catalysts and ion-exchange Nafion film. Besides, the electrons on surface will be decreased by the limited current density and high rotation speed [36].

In a typical ORR polarization curve of the catalyst, there are three parts where ORR kinetics are controlled in different ways: the kinetic controlled zone, the diffusion controlled zone and the mixed kinetic-diffusion controlled zone (Figure 2). In the initial kinetic controlled zone, the ORR is slow and the current density increases slightly with the decreased potential. In the following mixed controlled parts, the reaction accelerates and the current density increases with the dropping potential. While, the current density reaches a platform, whose value is determined by the test parameters. According to the Levich equation, the catalyst is able to achieve the limited current density of 5.78 mA/cm^2 (theoretical value) at 1600 r/min in 0.1 mol/L KOH at room temperature with sufficient amount of active sites [37]. The onset potential (E_{onset}) and the half-wave potential ($E_{1/2}$) are two important parameters for confining the activity of ORR catalysts. Commonly, the potential with 5% of the limited current density is defined as the E_{onset} [38]. The $E_{1/2}$ represents the potential with half of the limited current density. Besides, kinetic current density (J_K) is another factor in evaluating the ORR catalysts, which can be calculated by the Koutecky-Levich (K-L) equation:

$$\frac{1}{J} = \frac{1}{J_K} + \frac{1}{J_L} \tag{5}$$

where J is the current density, and J_L is the limited current density. The J_K at 0.9 or 0.95 V for Pt catalyst or Pt alloy catalyst is often compared. All of the potentials are usually compared with the commercial 20% Pt/C catalyst.

Electron transfer number (n) and the H_2O_2 production can be calculated by the RDE/RRDE results. The relative equations are listed below:

$$J_L = B\omega^{1/2} = 0.62nFC_0(D_0)^{2/3}v^{-1/6}\omega^{1/2} \tag{6}$$

$$4I_d = n(I_d + I_r / N) \tag{7}$$

$$H_2O_2\% = \left(2 * \frac{I_r}{N}\right) / \left(\frac{I_r}{N} + I_d\right) \tag{8}$$

where ω is the angular velocity, F is the faraday constant, C_0 is the oxygen bulk concentration, D_0 is the oxygen diffusion coefficient and v is the kinetic viscosity. I_d and I_r are the disk and current density, respectively. N is the current collection efficiency of the Pt ring.

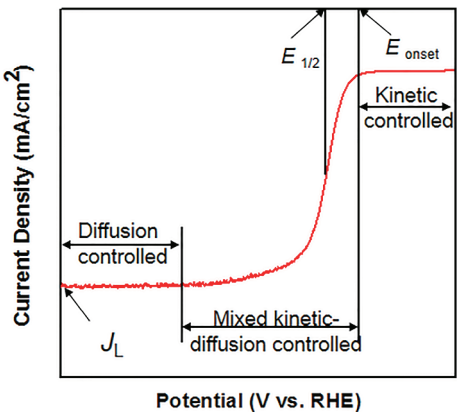

Figure 2 Typical ORR polarization curve (color online).

3 Non-noble metal-based catalysts for ORR

Non-noble metal-based catalysts have been widely explored due to its low cost, earth-abundant precursor and so on. For now, the ORR catalysts based on non-noble metal showed comparable activities to commercialized Pt/C catalysts as promising candidates for practical applications of fuel cells (Table 1). Commonly, the non-noble metal based ORR catalysts showed better durability in relative gentle conditions (e.g. 0.6 V vs. RHE in alkaline solution). Most of non-noble metal based catalysts were commonly available in alkaline electrolyte with good catalytic performance. Whereas, in acid electrolyte, the erosion process of non-noble metal leads to lower stability of the electrochemical catalyst, restricting the applications of non-noble metal based catalysts owing to the H^+-dominant condition in proton exchange membrane fuel cells (PEMFCs). In addition, the methanol crossover effect on non-noble metal catalysts is not as serious as platinum based catalysts, leading to a higher methanol tolerance. The catalytic activities and mechanisms of non-noble metal catalysts will be discussed in this section (Table 1). Among all types of non-noble metal catalysts, metal oxides present relative poor activities but high stabilities. While, the metal carbides/nitrides illustrate high catalytic performance even comparable to Pt/C only in base electrolyte. Moreover, due to the special electronic structures, the M–N/C species illustrated promising catalytic performance in both alkaline and acid conditions. However, the real active sites and mechanisms on the M–N/C catalysts are still debatable and will be discussed in the following section.

3.1 Metal oxide-based catalysts

Low cost and easily synthesized metal oxide is one important member of transition metal-based compounds, which has been proved active in ORR catalysts. However, most of the oxide suffered from low conductivity, dissolution and so on. Reducing the crystal to nanomaterials and combining the NPs

Table 1 ORR performance of non-noble metal-based catalysts in O_2 saturated 0.1 mol/L KOH

ORR catalyst	E_{onset} (V vs. RHE)	$E_{1/2}$ (vs. RHE)	n	Reference
Co_3O_4/N-rmGO	/	0.83	4	[20]
Fe_3O_4/N-GAs	0.77	/	~2	[39]
G–Co/CoO	/	0.78	/	[40]
FexN/NGA	0.95	/	4	[41]
TiN/CB	0.84	/	/	[42]
TiN/CNT–GR	0.83	/	/	[43]
Fe_2N@NPC-500	0.92	0.78	3.8	[44]
Fe_3C/NG-800 (in 0.1 mol/L $HClO_4$)	0.92	0.77	3.8	[45]
Fe_3C/C-700	1.05	0.83	/	[46]
Fe_3C/C-700 (in 0.1 mol/L $HClO_4$)	0.90	0.73	/	[46]
FeMoC-NG	0.87	/	4	[47]
Fe_3C@NCNT-800	1.05	0.81	/	[48]
Fe_3C@NCNT-800 (in 1 mol/L $HClO_4$)	0.92	0.72	/	[48]
Mn_3O_4	0.80	/	4	[49]
Fe–N/C-800	0.92	0.81	/	[50]
Co10-NMCV	0.83	0.78	4	[51]
Co SAs/N-C(900)	/	0.88	4	[52]
N/Co-doped PCP/NRGO	0.97	/	4	[53]
C–$MnFe_2O_4$	/	0.80	/	[23]
C–Fe_3O_4	/	0.61	/	[23]

with carbon substrates can help to improve the conductivity and avoid dissolution [54]. Reducing spinel and perovskite crystals into nano-sized clusters can help to improve the ORR activity. Besides, other non-noble metal oxide-based catalyst was also explored with ORR catalytic property.

3.1.1 Spinel (AB_2O_4)-based catalysts

Spinel (AB_2O_4) is a general class of minerals with equiaxed crystal system. In the spinel structure, 1/8 of the tetrahedral sites are occupied by A atoms, and 1/2 of the octahedral sites are occupied by B atoms. The spinel crystals were initially believed more active in oxygen evolution reaction (OER) than ORR in alkaline electrolyte [55]. However, Dai *et al*. [20] proposed a hybrid material of Co_3O_4 NPs on N-doped graphene (Co_3O_4/N-rmGO) as a highly active catalyst for the ORR (Figure 3(a, b)). The hybrid exhibited surprising highly ORR activity (with a positive ORR onset potential at 0.88 V relative to the RHE and higher cathodic currents) than the individual Co_3O_4 NPs or graphene oxide (Figure 3(c, d)). Besides, the Co_3O_4/N-rmGO exhibited ignorable decay in the alkaline electrolyte after even 25000 s continuous operation, which was superior to commercial Pt/C catalyst. The N component on the reduced graphene oxide (GO) was believed to serve as both the nucleation and catalytic-active sites. Even the mechanism of the ORR catalysts remained unclear, the synergistic coupling between the N-doped graphene and Co_3O_4 NPs was believed a must for the high performance. This work opened the relevant researches about the Co-based spinel crystal as well as other spinel-catalysts for ORR.

3.1.2 Perovskite (ABO_3)-based catalysts

Perovskite (ABO_3) is another important member of metal oxide (Figure 4(a)) [56]. In a typical perovskite crystal, the unit cell consists corner shared BO_6 octahedra together with A-site cations at the corner. The substitution of A, B cations and the generated oxygen deficiency have large influence on the electronic structure and coordination chemistry, which in turn confer the crystal with good ORR property [57]. Goodenough *et al*. [58] proposed the mechanism of the ORR on the perovskite crystal. It is proposed that the ORR process proceeded via an exchange between the adsorbed $O_2^-{}_{ads}$ solution species and the surface OH^- species. In this reaction proceeding, the surface OH^- species must be in high concentration and not too tightly bound to the surface.

The flexible perovskite structure can withstand large lattice mismatch and accommodate dopants on A and/or B site lattices, which provides more possibility for modified ORR catalysts. For example, Otagawa *et al*. [59] explored 18 substituted perovskites $La_{1-x}Sr_xMO_3$ (M=Ni, Co, Mn, Fe and so on). It was found that the catalytic property increased with a high occupancy of anti-bonding σ* orbital of M–OH. A volcano plot of catalytic activity versus M–OH bond was also proposed.

The mechanism of perovskite on ORR was also widely

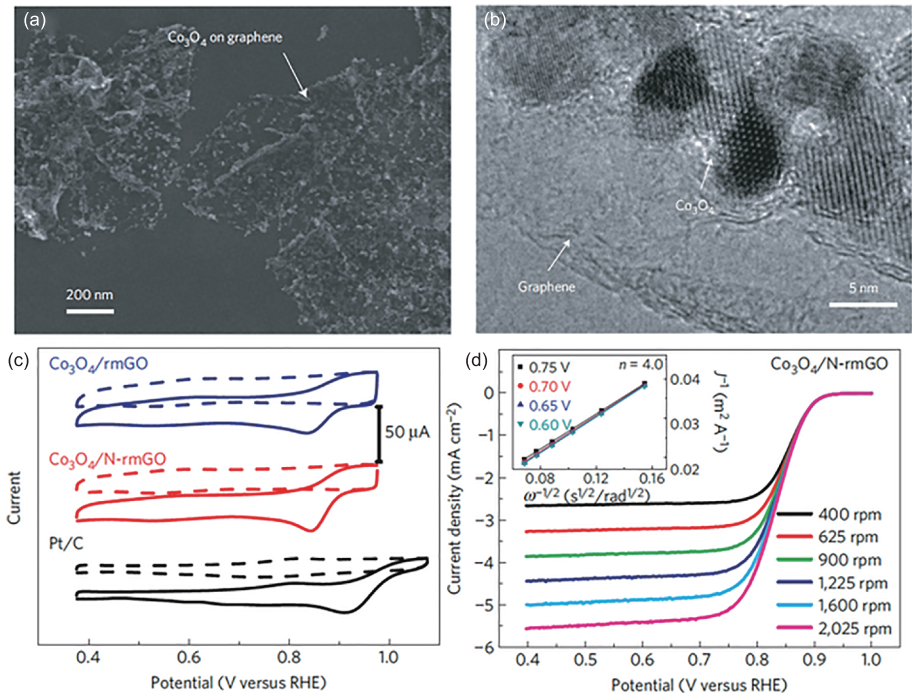

Figure 3 (a) Scanning electron microscopy image of Co_3O_4/N-rmGO hybrid; (b) high magnification transmission electron microscopy image of Co_3O_4/N-rmGO hybrid; (c) CV curves of Co_3O_4/rmGO hybrid, Co_3O_4/N-rmGO hybrid and Pt/C in O_2-saturated (solid line) or Ar-saturated 0.1 mol/L KOH (dash line); (d) Co_3O_4/N-rmGO hybrid (loading ~0.1 mg/cm^2) in O_2-saturated 0.1 mol/L KOH at the different rotation rates indicated. The insets showed Koutecky-Levich plots (J^{-1} versus $\omega^{-0.5}$) at different potentials. Adapted from Ref. [20] with permission from Nature Publishing Group (color online).

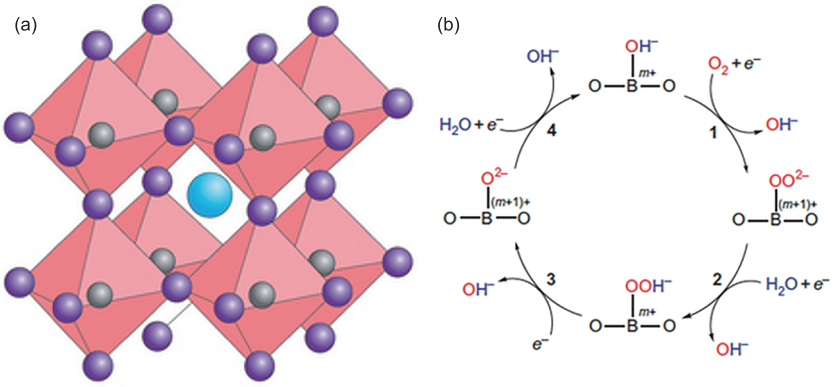

Figure 4 (a) Cubic perovskite crystal structure. Blue sphere was A, gray sphere was B and purple sphere was O. Adapted from Ref. [56] with permission from Nature Publishing Group. (b) ORR mechanism of perovskite. Adapted from Ref. [60] with permission from American Chemical Society (color online).

explored. In Figure 4(b), Shao-Horn *et al.* [60] proposed the ORR activity for perovskite correlated to σ*-orbital occupation and the extent of B-site transition metal-oxygen covalency. In the process of ORR in alkaline solution, the rate-limiting steps were the competition between the O_2^{2-}/OH^- displacement and the OH^- regeneration.

3.1.3 Other oxide-based catalysts

In addition, other non-noble metal oxides (MnO_2, Fe_2O_3, CoO and so on) were also studied of ORR catalytic property [61,62]. Manganese oxide of various structures were synthesized and explored for catalyzing ORR in alkaline solution [63]. It was shown that electro-catalytic activities were strongly dependent on the crystallographic structures, and followed an order of α-MnO_2>β-MnO_2>δ-MnO_2. When reaching 3 mA/cm^2, α-MnO_2 was at the potential of 760 mV close to 860 mV of the 20% Pt/C. The outstanding ORR activity of α-MnO_2 was proved due to the strongest O_2 adsorption capability. The onset potential of ORR on α-MnO_2 was at −0.14 to −0.13 V, larger than β-MnO_2 (−0.15 V) and δ-MnO_2 (−0.30 V). The half-wave potential for α-MnO_2 was between −0.20 and −0.24 V. In contrast, half-wave potentials of −0.30 and −0.34 V were for β-MnO_2 and δ-MnO_2.

3.2 Metal nitride-based catalysts

Metal nitrides have attracted much attention as efficient elec-

tro-catalysts for hydrogen evolution reaction (HER), ORR, OER and so on. High corrosion resistance and low electrical resistance make transition metal nitrides potential materials for energy conversion and storage applications [64]. In transition metal nitrides, nitrogen atoms are partly inserted in the interstitial positions of transition metals, leading to a narrow Fermi-gap [65]. The catalytic performance of transition metal nitrides are believed from the noble metal-like electronic structure [66]. Single and bi-metal nitrides have been proved with good ORR property.

3.2.1 Single-metal nitride-based catalysts

Single metal nitrides have been explored with good ORR property. In 1963, Trassatti *et al*. [67] reported the TiN electrode can be synthesized by treating the titanium electrode in nitrogen at high temperature. The TiN electrode showed oxygen reduction catalytic property in basic electrolyte. Lately, other metal nitride (Co_xN, Fe_xN_y, Mo_xN_y, W_xN_y) based ORR catalysts were also synthesized, combining with substrate (carbon nanotubes (CNTs), graphene, graphene aerogel) [41,44,68–72]. Recently, iron nitride-based on graphene aerogel was proposed with good catalytic property in alkaline electrolyte [41]. The iron nitride/nitrogen-doped graphene aerogel was fabricated by a facile two-step hydrothermal process of FePc and graphene oxide. The resulting iron nitride NPs were uniformly distributed on the 3D mesoporous graphene aerogel with a diameter of about 5 to 20 nm. The synergistic effect between iron nitride and the graphene substrates promoted the ORR. The onset potential of the hybrid was close to the commercial Pt/C catalyst and the charge transfer resistance was much lower than the individual graphene aerogel, iron nitride and their physical mixture. Besides, the catalysts showed better stability in alkaline electrolyte than the commercial Pt/C and proceeded a direct 4-electron transfer process. What is more, the large surface area and porosity were also of vital importance for the good catalytic property.

In addition to the RDE tests, some test on PEMFCs are also proceeded to explore the ORR property on non-noble metal nitride-based catalysts. Wang [73] proposed a single-phase *fcc* structure of β-W_2N (2−7 nm) nanocrystals on Vulcan XC-72R support (β-W_2N/C), as shown in Figure 5(a, b). Linear scan voltammogram of β-W_2N/C showed its ORR activity. In Figure 5(c), single cell tests were also achieved with the as-prepared W_2N/C (18 wt% W) as the cathode electro-catalyst from 60 to 80 °C. At the current density of 100 mA/cm^2, the cell voltage at 80 °C is 0.367 V, of which the maximum power density is 39.2 mW/cm^2. Stability test of the single cell was also carried out at the current density of 120 mA/cm^2, which showed almost no decay for 80 h (Figure 5(d)).

3.2.2 Bi-metal nitride-based catalysts

More recently, bimetallic nitrides have also been explored for finding more active metal nitride-based catalysts. It is believed the synergistic effect of the bi-metal nitride could promote the ORR catalytic property. Cui *et al*. [74] proposed the synthesis of mesoporous cobalt molybdenum nitride

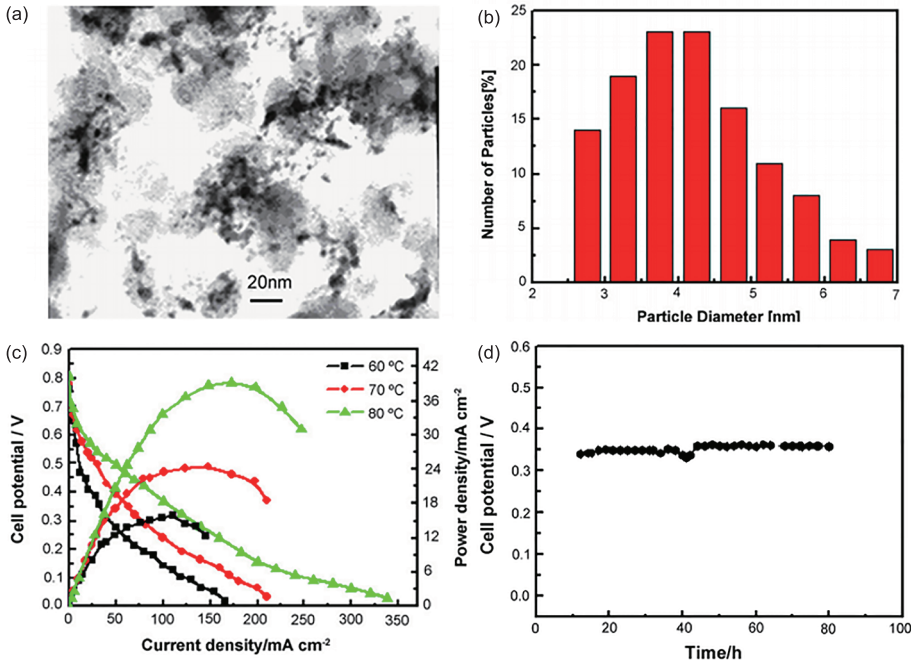

Figure 5 (a) TEM analysis of W_2N/C (18 wt%) catalyst and (b) corresponding particle size distribution; (c) polarization curves at different cell temperatures of the single cell with the W_2N/C (18 wt% W) as the cathode catalyst; (d) stability test of the catalyst at the constant current density. Adapted from Ref. [73] with permission from Elsevier (color online).

(Co_3Mo_3N) by a co-precipitation method followed by ammonia annealing treatment (Figure 6(a)). More active-site exposure was generated by the well-designed mesoporous structure (Figure 6(b, c)) and the intrinsically electronic configuration resulted in excellent ORR catalytic performance in alkaline solution. The assembled Li-O_2 battery showed promising discharging capacity and cycling stability (Figure 6(d)).

3.3 Metal carbide-based catalysts

Initially, metal carbides were used as support for ORR catalysts for its high electronic conductivity and stability [75]. Especially, tungsten carbide (W_xC) was widely used as the catalyst support for its Pt-like surface electronic properties. For example, palladium and Fe on nanocrystalline tungsten carbide (PdFe-WC/C) was obtained with WC as support [76]. In 0.5 mol/L H_2SO_4, PdFe-WC/C showed comparable catalytic property to that of commercial Pt/C catalyst, which was believed from the synergistic effect of Pd, Fe and WC base. In addition, non-noble metal carbide based ORR catalysts were also synthesized.

3.3.1 Single-metal carbide-based catalysts

Transition metal carbide-based nanomaterials have been widely applied as ORR catalysts, including the single metal carbide-based nanomaterials and bi-metal carbide-based nanomaterials [46,77]. Especially, iron carbides have caused intensive attention for its enhanced ORR activity, especially the one with Fe/C core/shell structure. Usually, iron ions could be reduced into metallic NPs by carbon during the heating process. Lately, carbon atoms diffused into the interstitial void of metallic iron to form iron carbide. At the same time, carbon component in precursor can be catalyzed into graphitic carbon shell, which will protect the metallic core from corrosion and decay of catalytic property [78]. Iron carbide (especially Fe_3C)-based nanomaterials have been proved with good ORR performance by series works. A facile heat-treated core/shell Fe/Fe_3C-C nanorods have been synthesized from cyanamide and $FeCl_3$ [79]. The Fe/Fe_3C NPs with an average diameter of 20 to 30 nm were encased in the nitrogen-doped graphitic carbon shell. Compared with Pt/C, the Fe/Fe_3C@C nanorods showed improved activity and enhanced kinetics with reduced cost in neutral solutions. In MFCs test, the as-developed catalysts showed long-term stability. It is worth noting that the MFC with Fe/Fe_3C-based catalysts showed remarkable performance compared with the one with commercial Pt/C. Iron carbide encased in dense graphitic carbon stands out in catalyzing ORR process in acid electrolyte, which can be achieved easily by annealing process. It is believed that the Fe_3C NPs play an important role in activating the outer graphitic layers for ORR. Besides, the outer graphitic shells can stabilize the inner iron carbide NPs to protect them from corrosion and decay.

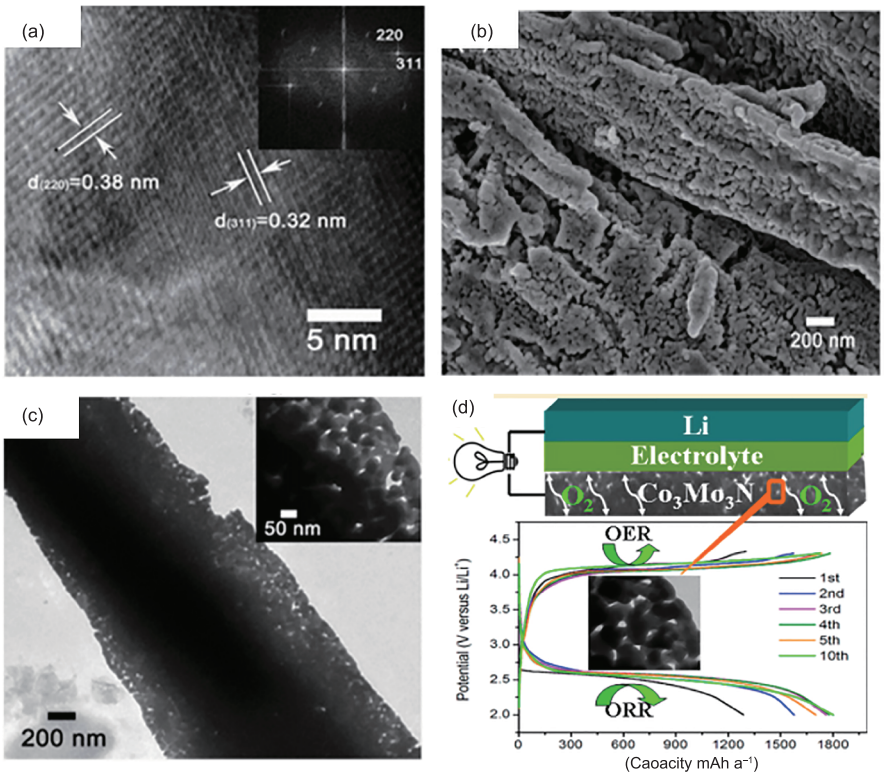

Figure 6 (a) HRTEM image and the corresponding FFT patterns (inset) of Co_3Mo_3N; (b) scanning electron microscope (SEM) image of Co_3Mo_3N; (c) TEM images of Co_3Mo_3N; (d) scheme of Li-O_2 battery, discharge and charge voltage profiles of the Co_3Mo_3N based cell at various cycles at a current density of 0.1 mA/cm^2 in the voltage windows between 2.0 and 4.3 V. Adapted from Ref. [74] with permission from the American Chemical Society (color online).

3.3.2 Bi-metal carbide-based catalysts

Bi-metallic carbide-based catalysts are believed to be efficient for ORR. The synergistic effect of multi-metal and substrate can promote the electron transfer for reaction, thus accelerating the ORR process. Shen *et al*. [47] proposed a bi-metal carbide-based catalyst of Fe and Mo with highly catalytic property. The as-prepared FeMo carbide-based catalysts showed excellent electro-catalytic activities for ORR in alkaline electrolyte, with high onset potential (−0.09 V vs. Ag/AgCl), nearly 4-electron transfer number. The catalytic role of individual content was also compared by varying the Fe/Mo weight ratios. The catalytic order (FeMo (1:3) Carbide/NG-800 (3.6 mA/cm^2)>FeMo (3:1) Carbide/NG-800 (3.2 mA/cm^2)>Mo Carbide/ NG-800(2.7 mA/cm^2)>Fe Carbide/NG-800 (2.5 mA/cm^2)) indicated the higher catalytic performance of bi-metal carbide-based catalysts than that of single one. The outstanding ORR performance was due to the synergistic effect of the well-dispersed transition metal carbide NPs and N-doped graphene. It is worth noting that the N-doping is found to play a vital role in improving the ORR performance by promoting the electron transfer and increasing the density of active sites.

3.4 M–N/C-based catalysts

The macro-cyclic structure based ORR catalysts can date back to the year of 1964, when Jasinski [80] reported ORR catalyst based on macro-cyclic structure with M–N coordination for the first time. Subsequently, further researches on the M–N_4 macro-cycle were proceeded, finding that such structures were not stable in acid electrolyte. Later, heat treatment of M–N_4 macro-cycles in an inert atmosphere was proposed to improve the ORR activity and stability in 1970 [81,82]. Gupta *et al*. [83] reported the ORR catalyst with non-M–N_4-macrocycles as nitrogen source, leading to more researches on preparing ORR catalysts with cheaper and more common inorganic salts as precursors. In the subsequent studies, various precursors were used for preparing ORR catalysts, such as organometallics, N_x-metal chelates and some common inorganic salts [84,85]. It was commonly accepted that heat-treated catalysts, especially the ones with precursors of M–N chelation, were good catalysts in both acid and alkaline electrolyte. Whereas, it was found out that when the metallic center was not chemically bound to the macro-cycle after heat-treating the M–N_4 macro-cyclic catalyst, it still processed good ORR property [86]. As a result, there are still lots of conflicts about whether the M–N_4 structure was totally destroyed after heat-treatment and what exactly the active sites of the ORR are.

Nanostructured M–N/C catalysts were also developed with high ORR catalytic property. Pyrolysis of cheap and common precursors containing M, N and C is one of the most cost-effective methods, which can produce catalysts containing M, N and C were believed with effective M–N/C active sites. A one-pot, large-scale protocol for preparing 1D bamboo-like carbon nanotube/Fe_3C nanoparticle hybrid for ORR catalysts were proposed [87]. In Figure 7(a), the ORR catalysts were prepared by directly annealing the mixture of P123, melamine, and Fe $(NO_3)_3$ in an inert atmosphere. The 1D bamboo-like CNTs could provide more exposure of the active sites. The Fe_3C NPs encased by the CNTs could form more M–N/C active sites, promoting the ORR activity (Figure 7(b–g)). The half-wave potential of the catalyst was 0.861 V (vs. RHE) in 0.10 mol/L KOH solution, which was even more positive than the commercial Pt/C catalyst. The ORR activity of the catalyst was also comparable to the commercial Pt/C catalyst in acid electrolyte. Higher stability and better methanol tolerance were also observed for the catalyst.

Whether the M is part of the active sites or just catalyzes the formation of the active sites is one of the hot debates. Scherson *et al*. [88] proposed that the M component was not the active site but only catalyst to form the active sites. *In situ* Fe K-edge X-ray near-edge structure showed that iron sites in the thermally activated material were quite different from those in the M–N_4 environment of the intact macro-cycle. Subsequently, Ozaki *et al*. [89] revealed the nature of active sites of the catalysts by X-ray adsorption fine structure analysis and hard X-ray photoemission spectroscopy. It was found out that the Co content existed in the dorm of metallic Co in the Co–N–C catalysts and the catalysts still remained effective after removing the Co by acid washing. The authors held the idea that M-component was not part of the active sites.

However, there are amounts of researches proving the M part played important roles in activating the catalysts as part of the active sites. Fe_3C/C was synthesized a facile pyrolyzing process of ferrocene and cyanamide in nitrogen. The Fe_3C NPs were encapsulated in graphitic carbon layers [46]. In RDE test, the Fe_3C/C-700 catalyst exhibited a high onset potential (0.90 V) and a half-wave potential at 0.73 V in 0.1 mol/L $HClO_4$, both of which were comparable to commercial Pt/C. After the ball-milling and acid leaching, the micro-spherical morphologies of the catalysts were destroyed and Fe_3C particles were almost removed (Fe_3C/C-700L). As a consequence, the corresponding sample lost the magnetic property, illustrating the remove of Fe_3C NPs. The non-ignorable potential shift between the Fe_3C/C-700BL and Fe_3C/C-700 proved the role of M in catalyzing ORR.

The real active site of the M–N/C-based ORR catalysts is still a debated issue [90]. Wei *et al*. [91] explored the ORR catalytic performance of a highly active Fe–N–C ORR catalyst containing Fe–N_x coordination sites and Fe/Fe_3C nanocrystals. It is convinced that the interaction between metallic iron and Fe–N_4 coordination structure favored the adsorption of oxygen molecule. Zelenay *et al*. [92]

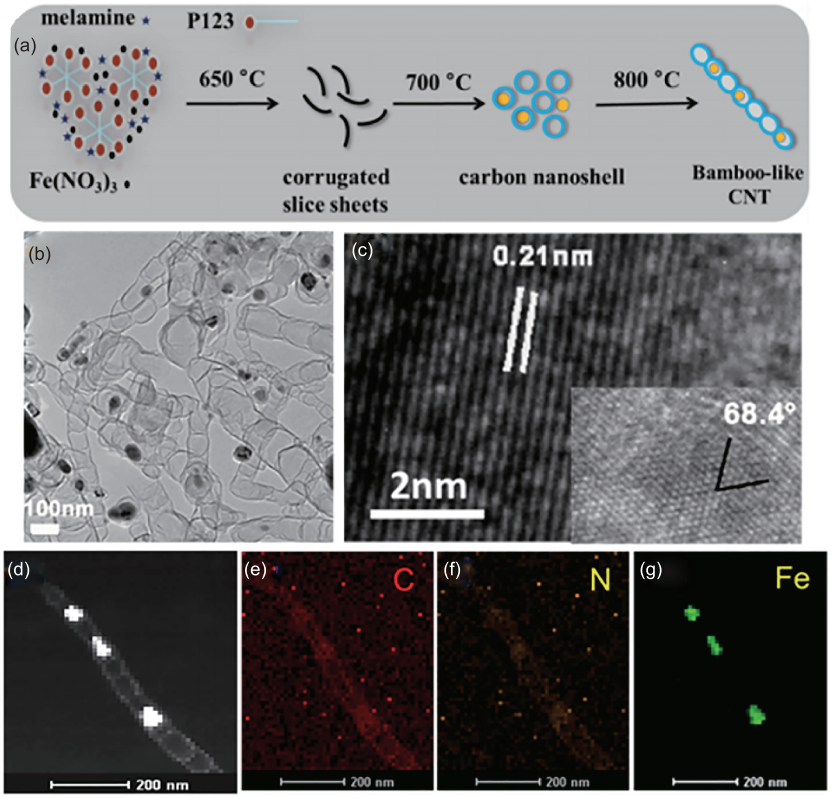

Figure 7 (a) Illustration of the formation of the bamboo-like carbon nanotube/Fe_3C nanoparticle; (b) TEM image, (c) HRTEM, (d) high angle annular dark field scanning transmission electron microscopy (HAADFSTEM), and (e–g) its mapping images of the resultant bamboo-like carbon nanotube/Fe_3C nanoparticle. Adapted from Ref. [87] with permission from the American Chemical Society (color online).

illustrated the performance of H_2-air fuel cells with Fe–N–C catalysts with various nitrogen precursors. DFT calculation and the current densities recorded showed the catalysts with edge-hosted FeN_4 sites were likely the major contributors. It is widely accepted that the M–N coordination is a must for highly active M–N/C ORR catalysts.

The ORR property of the catalysts was related to the active sites as well as micro-porosity, pyridinic nitrogen content and so on. One study on M–N chelates of different metal (M=Fe, Co, Cu, Zn) showed that the ORR activity of different M–N/C catalysts increased in the order of H≈Zn<Cu<Co<Fe (Figure 8(a)) [93]. Different M ions coordinated to N affected the morphology, structure and physical-chemical property of the catalysts. Micro-porosity was one important factor for ORR catalysts. Increasing the porosity by heat treatment in reactive gases such as NH_3 could increase the porosity, thus led to higher accessibility to oxygen. Content of pyridinic nitrogen could also influence the ORR property. It was evident that transition metal in precursor could fix nitrogen, with the order of Zn>Cu>Co>Fe. In addition, variety of nitrogen was also affected by the transition metal, leading to influence on ORR activity (Figure 8(b)). To conclude, micro-porosity, pyridinic nitrogen content were all related to the ORR property.

4 Carbon-based ORR catalyst

Compared to other non-precious metal catalyst group, carbon catalysts, including amorphous carbon, CNTs, 2D graphene and graphite, are more promising for the practical application due to the low cost, high conductivity and large surface area [94]. Generally, the ORR performance of carbon based materials could be boosted by the heteroatom doping, as the heteroatom dopants could improve the excellent electric conductivities, mechanical flexibilities, superior surface areas and sufficient stabilities [95]. Therefore, the carbon materials are considered to replace Pt in the future for fuel cell and other electrochemical energy application. Specifically, the N [96], P [97], S [98], B [99] *et al*. are often chosen to be doped into carbon framework for triggering the ORR performance. It is worth noting that the carbon-based ORR catalyst is not subjected to the harsh condition of both base and acid solution, but suffers from the oxidation from high potential. What is more, the carbon-based catalyst also presented high methanol tolerance. Therefore, it cannot be questioned that the following experiment and simulation investigations of the heteroatom dopants in carbon materials could guide the researchers to obtain the high performance carbon-based catalyst.

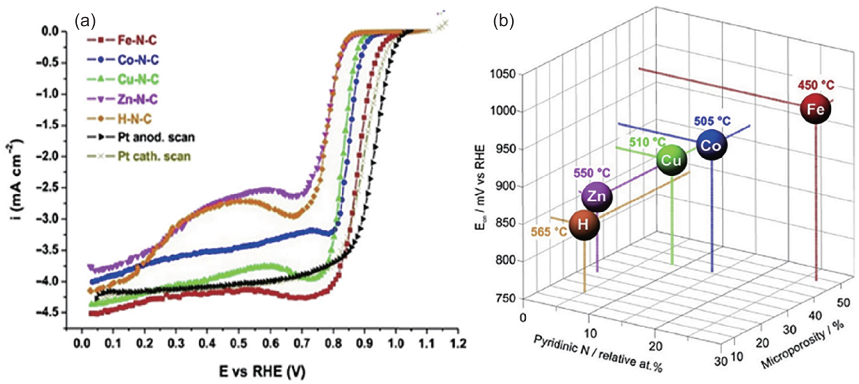

Figure 8 (a) Staircase voltammetry recorded at 900 r/min RDE rotation speed of catalysts with different metal; (b) graph summarizing the factors that influence the ORR activity in alkaline conditions (measured in terms of onset potential): pyridinic nitrogen content, micro-porosity, and dehydrogenation start temperature during pyrolysis of the precursor. Adapted from Ref. [93] with permission from Elsevier (color online).

4.1 Nitrogen-doped carbon catalyst

As a common non-metal dopant, nitrogen can be doped into several locations within the carbon structure, resulting in effective ORR activities. Dai and co-workers [96] reported a vertically aligned nitrogen-containing CNTs which obtained a much better ORR catalytic activity, long-term operation stability, and tolerance to methanol than 20 Pt/C. It delivered a steady-state output potential of −80 mV and a current density of 4.1 mA/cm^2 at −0.22 V, compared with −85 mV and 1.1 mA/cm^2 at −0.20 V for a Pt/C electrode. In general, the five available valence electrons present in nitrogen could form sp^2-like hybridization between N and C atoms into C–N bonds, which were considerably polarized owing to the larger electronegativity of N than C and became active sites for O_2 adsorption [96]. Comparable atomic sizes of N and C allow the N atoms dope into C planes by three types including "pyridinic", "pyrrolic" and "graphitic" N. As shown in Figure 9(a), pyridinic N is located at the edge sites and possesses two sp^2 carbons [100]. Therefore, it provides the graphitic π system with one pπ electron. In contrast, the graphitic nitrogen is able to provide two pπ electrons. Additionally, the pyrrolic nitrogen atom in the five-sided ring is thermally unstable. These three types of N-doping location could be distinguished by N peak in X-ray photoelectron spectroscopy (XPS) results, as shown in Figure 9(b), in which the N1s peak has three components centered at 398.2, 400.3 and 401.5 eV, corresponding to pyridinic, pyrrolic, and graphitic N, respectively [100].

Ruoff and co-workers [101] investigated the effect of the bonding state of the N atom in graphene on the selectivity and catalytic activity for ORR. It has been found that the electro-catalytic activity of the catalyst is dependent on the graphitic N content which determines the limiting current density. While the pyridinic N content improves the onset potential for ORR. However, the total N content in the graphene-based non-precious metal catalyst does not play an important role in the ORR process. Recently, the various N-doped C has been widely investigated to fulfil its potential as ORR catalysts. Yu *et al*. [102] utilized a hydrothermal process with oxidized CNTs, GO, and ammonia as precursors to synthesize a N-doped graphene and N-doped CNTs nanocomposite (N-doped graphene/CNT composites) catalyst, in which ammonia is not only as nitrogen sources to obtain the N-doped graphene but also N-doped CNTs. The value of onset potential was −140 mV for N-doped graphene/CNT composites which was much more positive than those of the N-doped graphene, N-doped CNTs, graphene/CNT composites and directly mixed product of GO and oxidized CNTs. Since the N-doped graphene and N-doped CNT catalysts have shown promising ORR activity individually, some interest has sprouted up to develop N-doped carbon catalysts with the embedded N sources and one-pot methods [103,104]. N-doped porous carbons have been synthesized by using a zeolite-type nanoscale metal-organic frameworks as a self-sacrificing template, which simultaneously acted as both the carbon and nitrogen sources in a facile carbonization process [105]. The obtained high ORR activities were ascribed to the synergetic contributions of the abundant active sites with high graphitic N portion, high surface area and porosity, and the high degree of graphitization [105]. Although, the N-doped carbon materials have exhibited significantly improved ORR activity, unfortunately, it is not possible to completely control nitrogen-doping sites in carbon nanomaterials.

4.2 Other atom-doped graphene

Other heteroatoms such as boron-, sulfur- and phosphorous-doped carbon materials also have been studied in terms of their catalytic activity for ORR. Hou *et al*. [97] reported a phosphorus-doped graphene as shown in Figure 10(a) synthesized via low-cost and scalable thermal annealing method for the synthesis of P-doped graphene (PG) using GO and triphenylphosphine as carbon and phosphorus sources, respectively. The energy dispersive X-ray (EDX) spectrum indicated the presence of O (2.02 at%) and P (1.32 at%)

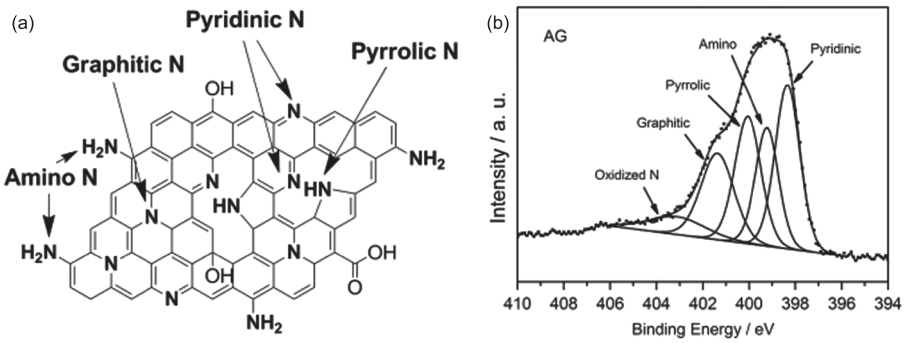

Figure 9 (a) Nitrogen doping into carbon plane at different location; (b) N 1s peak of N-doped graphene in XPS spectra. Adapted from Ref. [100] with permission from Elsevier (color online).

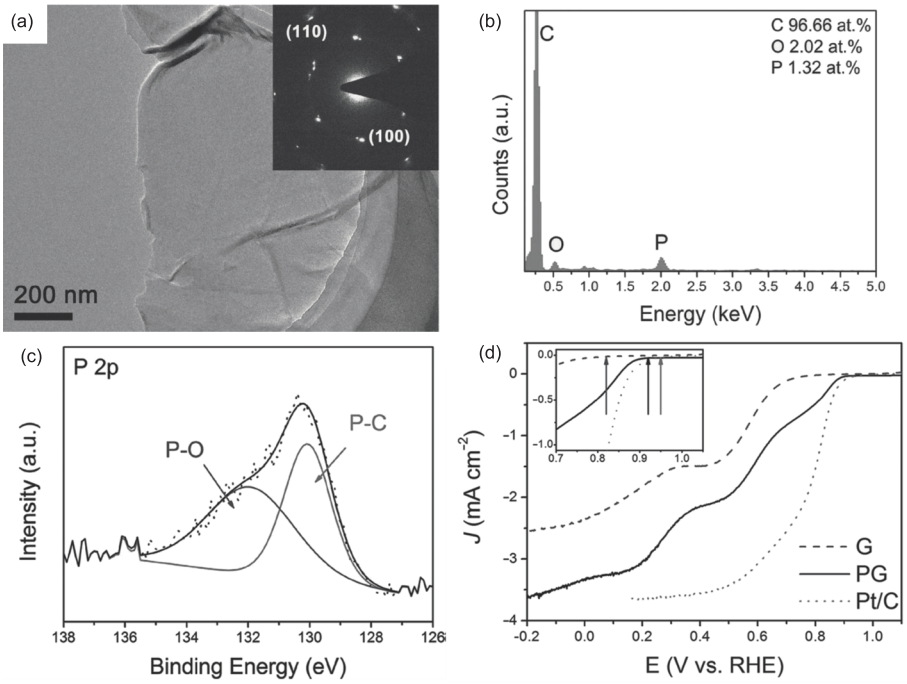

Figure 10 (a) TEM image of PG and the corresponding SAED pattern (inset); (b) EDX spectrum of P-doped graphene; (c) the high-resolution P 2p XPS spectrum of P-doped graphene; (d) LSV curves of graphene, P-doped graphene and Pt/C in an O_2-saturated 0.1 mol/L KOH solution at a scanning rate of 10 mV/s and a rotation speed of 1600 r/min. Inset of (d) shows the onset potential of graphene, P-doped graphene and Pt/C. Adapted from Ref. [97] with permission from Wiley.

elements (Figure 10(b)). The P 2p peak in XPS results confirmed that the P–C and P–O bond exist in P-doped graphene in Figure 10(c, d). The resultant PG showed remarkable catalytic activity with onset potential of ca. 0.92 V. Also, from the K-L equation, it was indicated that the ORR proceeded via a combination of two-electron and four-electron pathway [97]. Although the P-doped graphene shown an outstanding tolerance to methanol crossover effect and excellent long-term stability compared with Pt/C electrode, its ORR performance is still not comparable to Pt/C catalyst.

Müllen and co-works [98] investigated the comparison the ORR activities between S- and N-doped graphene. The studies proved that sulphur could be doped into graphene sheets in a major form of thiophene-like S. The electro-catalytic activity of S-doped graphene is strongly dependent on the annealing temperature, resulted from the different states of S–C bonds. However, it is found that the kinetic current density of S-doped graphene (5.3 mA/cm^2) is significantly lower than that of N-doped graphene (7.8 mA/cm^2). The worse performance is due to that: 1) S–C bonds are predominately at the edges; and 2) there are defect sites of S-doped graphene, which results in the lower content and inhomogeneous distribution of sulfur in S-doped graphene compared to that of N in N-doped graphene. Although the other heteroatoms-doped carbon materials have been developed which are of fundamental importance to understand the effects on changes of electronic and geometric structure of carbons from the dopants [85]. Unfortunately, no significantly improvement of

ORR performance has been obtained so far by doping these heteroatoms beyond nitrogen.

4.3 Multi-elements co-doped carbon catalyst

Most of reports show excellent ORR performance of heteroatom-doped carbon-based electrocatalysts in alkaline media, but only very few studies show a good performance in acid media as well. Even if previously reported N-doped metal-free carbons exhibited a good performance in acid media, their performance fast declined after several cycles due to degradation of the carbon matrix. To further improve the ORR activities, the addition of non-precious metals as secondary dopants has been induced into the N-doped carbon-based materials, leading to that catalysts exhibit a higher activity, long-term stability, and better tolerance to poisons than only N-doped carbons.

Qiao and co-workers [106] reported a B, N co-doped graphene via a two-step doping method by calcining GO with NH_3 and subsequently H_3BO_3 to dope the N and B respectively. According to the experimental data and DFT simulation, the co-doped catalyst illustrated excellent activity, good methanol tolerance and excellent long-term stability in an alkaline medium compared with singly B- or N-doped graphene. Dai *et al*. [107] prepared N, P co-doped carbon networks by pyrolyzing the super-molecular aggregate of self-assembled melamine, phytic acid, and GO, which displayed remarkably high ORR catalytic activity in acid and base electrolyte. The N and P co-dopants could induce charge redistribution to enhance the ORR activity. The enhanced ORR performance was reported mainly due to the synergistic effects that arise between the doped heteroatoms which would result in a larger asymmetrical spin and higher charge density than that can be achieved by single heteroatom doping.

5 Conclusions

Numerous efforts have been made to explore ORR catalysts with low cost, high performance and earth-abundant sources. This work has systematically reviewed and discussed the design and synthesis of potential noble metal-free nanocatalysts, including transition metal oxides, transition metal carbides, and transition metal nitrides-based nanomaterials, M–N/C species and heteroatom-doped carbon materials. The M–N/C species are considered as the promising ORR catalysts with high performance, stability and selectivity and so on, although the reported noble metal-free ORR catalysts showed comparable performance with commercial Pt/C catalysts. Whereas, the non-noble metal catalysts still need further improvements: (1) Higher stability in harsh condition should be addressed. ORR catalysts in practical utilization are normally exposed to highly oxidative and corrosive environments, where transition metal-based nanomaterials and metal-free nanomaterials are less stable. (2) Active sites density is supposed to be improved for improving the volumetric current. (3) The mechanism to improve the ORR performance of noble metal-free catalysts in MFCs is still debatable. The ORR process in micro-environment at electrode surface in practical fuel-cell is more complicated than that of electrochemical cell. (4) The structure-activity relationship of noble metal-free nanomaterials has not been well built. The rather complicated structure of noble metal-free catalysts makes it more difficult to explore the structure-activity relationship than noble metal catalysts. (5) Low-cost precursors and more facile synthesis are needed, since the practical ORR catalysts need facile synthesis method and low-cost for commercial production.

In addition, the development in nanomaterial, nanochemistry and characterization method may provide more convenience for figuring out the above questions, such as *in-situ* researches, and valence state.

Acknowledgments This work was supported by the State key Project of Research and Development of China (2016YFA0200102, 2017YFA0206301), the National Natural Science Foundation of China (51590882, 51631001, 51672010), and NSFC-RGC Joint Research Scheme (51361165201).

Conflict of interest The authors declare that they have no conflict of interest.

1 Steele BCH, Heinzel A. *Nature*, 2001, 414: 345–352
2 Larminie J, Dicks A, McDonald MS. *Fuel Cell Systems Explained*. Chichester, UK: J Wiley, 2003
3 Nørskov JK, Rossmeisl J, Logadottir A, Lindqvist L, Kitchin JR, Bligaard T, Jónsson H. *J Phys Chem B*, 2004, 108: 17886–17892
4 Morozan A, Jousselme B, Palacin S. *Energ Environ Sci*, 2011, 4: 1238–1254
5 Vielstich W, Yokokawa H, Gasteiger HA. *Handbook of Fuel Cells: Fundamentals Technology and Applications*. Weinheim: John Wiley & Sons, 2009
6 Gasteiger HA, Kocha SS, Sompalli B, Wagner FT. *Appl Catal B-Environ*, 2005, 56: 9–35
7 Paulus UA, Schmidt TJ, Gasteiger HA, Behm RJ. *J Electroanal Chem*, 2001, 495: 134–145
8 Bing Y, Liu H, Zhang L, Ghosh D, Zhang J. *Chem Soc Rev*, 2010, 39: 2184–2202
9 Wang C, Daimon H, Lee Y, Kim J, Sun S. *J Am Chem Soc*, 2007, 129: 6974–6975
10 Wang C, Daimon H, Onodera T, Koda T, Sun S. *Angew Chem Int Ed*, 2008, 47: 3588–3591
11 Stamenkovic VR, Fowler B, Mun BS, Wang G, Ross PN, Lucas CA, Marković NM. *Science*, 2007, 315: 493–497
12 Huang X, Zhao Z, Cao L, Chen Y, Zhu E, Lin Z, Li M, Yan A, Zettl A, Wang YM, Duan X, Mueller T, Huang Y. *Science*, 2015, 348: 1230–1234
13 He DS, He D, Wang J, Lin Y, Yin P, Hong X, Wu Y, Li Y. *J Am Chem Soc*, 2016, 138: 1494–1497
14 Li M, Zhao Z, Cheng T, Fortunelli A, Chen CY, Yu R, Zhang Q, Gu L, Merinov BV, Lin Z, Zhu E, Yu T, Jia Q, Guo J, Zhang L, Goddard Iii WA, Huang Y, Duan X. *Science*, 2016, 354: 1414–1419

15 Bu L, Zhang N, Guo S, Zhang X, Li J, Yao J, Wu T, Lu G, Ma JY, Su D, Huang X. *Science*, 2016, 354: 1410–1414
16 Bu L, Guo S, Zhang X, Shen X, Su D, Lu G, Zhu X, Yao J, Guo J, Huang X. *Nat Commun*, 2016, 7: 11850
17 Lefèvre M, Proietti E, Jaouen F, Dodelet JP. *Science*, 2009, 324: 71–74
18 Wu G, More KL, Johnston CM, Zelenay P. *Science*, 2011, 332: 443–447
19 Peng H, Mo Z, Liao S, Liang H, Yang L, Luo F, Song H, Zhong Y, Zhang B. *Sci Rep*, 2013, 3: 1765
20 Liang Y, Li Y, Wang H, Zhou J, Wang J, Regier T, Dai H. *Nat Mater*, 2011, 10: 780–786
21 Lee K, Zhang L, Lui H, Hui R, Shi Z, Zhang J. *Electrochim Acta*, 2009, 54: 4704–4711
22 Easton EB, Yang R, Bonakdarpour A, Dahn JR. *Electrochem Solid-State Lett*, 2007, 10: B6
23 Zhu H, Zhang S, Huang YX, Wu L, Sun S. *Nano Lett*, 2013, 13: 2947–2951
24 Ponce J, Rehspringer JL, Poillerat G, Gautier JL. *Electrochim Acta*, 2001, 46: 3373–3380
25 Yu D, Zhang Q, Dai L. *J Am Chem Soc*, 2010, 132: 15127–15129
26 Yang DS, Bhattacharjya D, Inamdar S, Park J, Yu JS. *J Am Chem Soc*, 2012, 134: 16127–16130
27 Zheng Y, Jiao Y, Chen J, Liu J, Liang J, Du A, Zhang W, Zhu Z, Smith SC, Jaroniec M, Lu GQM, Qiao SZ. *J Am Chem Soc*, 2011, 133: 20116–20119
28 Marković NM, Schmidt TJ, Stamenković V, Ross PN. *Fuel Cells*, 2001, 1: 105–116
29 Wang JX, Inada H, Wu L, Zhu Y, Choi YM, Liu P, Zhou WP, Adzic RR. *J Am Chem Soc*, 2009, 131: 17298–17302
30 Wu J, Yang H. *Acc Chem Res*, 2013, 46: 1848–1857
31 Holade Y, Sahin N, Servat K, Napporn T, Kokoh K. *Catalysts*, 2015, 5: 310–348
32 Lim DH, Wilcox J. *J Phys Chem C*, 2012, 116: 3653–3660
33 Stacy J, Regmi YN, Leonard B, Fan M. *Renew Sustain Energ Rev*, 2017, 69: 401–414
34 Bidault F, Brett DJL, Middleton PH, Brandon NP. *J Power Sources*, 2009, 187: 39–48
35 Gloaguen F, Andolfatto F, Durand R, Ozil P. *J Appl Electrochem*, 1994, 24: 863–869
36 Treimer S, Tang A, Johnson D . *Electroanalysis*, 2002, 14: 165
37 Davis RE, Horvath GL, Tobias CW. *Electrochim Acta*, 1967, 12: 287–297
38 Zhou X, Qiao J, Yang L, Zhang J. *Adv Energ Mater*, 2014, 4: 1301523
39 Wu ZS, Yang S, Sun Y, Parvez K, Feng X, Müllen K. *J Am Chem Soc*, 2012, 134: 9082–9085
40 Guo S, Zhang S, Wu L, Sun S. *Angew Chem*, 2012, 124: 11940–11943
41 Yin H, Zhang C, Liu F, Hou Y. *Adv Funct Mater*, 2014, 24: 2930–2937
42 Chen J, Takanabe K, Ohnishi R, Lu D, Okada S, Hatasawa H, Morioka H, Antonietti M, Kubota J, Domen K. *Chem Commun*, 2010, 46: 7492–7494
43 Youn DH, Bae G, Han S, Kim JY, Jang JW, Park H, Choi SH, Lee JS. *J Mater Chem A*, 2013, 1: 8007–8015
44 Huang X, Yang Z, Dong B, Wang Y, Tang T, Hou Y. *Nanoscale*, 2017, 9: 8102–8106
45 Liang HW, Wei W, Wu ZS, Feng X, Müllen K. *J Am Chem Soc*, 2013, 135: 16002–16005
46 Hu Y, Jensen JO, Zhang W, Cleemann LN, Xing W, Bjerrum NJ, Li Q. *Angew Chem Int Ed*, 2014, 53: 3675–3679
47 Chen M, Liu J, Zhou W, Lin J, Shen Z. *Sci Rep*, 2015, 5: 10389
48 Zhong G, Wang H, Yu H, Peng F. *J Power Sources*, 2015, 286: 495–503
49 Gorlin Y, Chung CJ, Nordlund D, Clemens BM, Jaramillo TF. *ACS Catal*, 2012, 2: 2687–2694
50 Lin L, Zhu Q, Xu AW. *J Am Chem Soc*, 2014, 136: 11027–11033
51 Li M, Bo X, Zhang Y, Han C, Nsabimana A, Guo L. *J Mater Chem A*, 2014, 2: 11672–11682
52 Yin P, Yao T, Wu Y, Zheng L, Lin Y, Liu W, Ju H, Zhu J, Hong X, Deng Z, Zhou G, Wei S, Li Y. *Angew Chem Int Ed*, 2016, 55: 10800–10805
53 Hou Y, Wen Z, Cui S, Ci S, Mao S, Chen J. *Adv Funct Mater*, 2015, 25: 872–882
54 Ishihara A, Ohgi Y, Matsuzawa K, Mitsushima S, Ota K. *Electrochim Acta*, 2010, 55: 8005–8012
55 Trasatti S. *Electrochim Acta*, 1984, 29: 1503–1512
56 Green MA, Ho-Baillie A, Snaith HJ. *Nat Photon*, 2014, 8: 506–514
57 Wang G, Xu T, Wen S, Pan M. *Sci China Chem*, 2015, 58: 871–878
58 Goodenough JB, Manoharan R, Paranthaman M. *J Am Chem Soc*, 1990, 112: 2076–2082
59 Bockris JOM. *J Electrochem Soc*, 1984, 131: 290–302
60 Suntivich J, Gasteiger HA, Yabuuchi N, Nakanishi H, Goodenough JB, Shao-Horn Y. *Nat Chem*, 2011, 3: 546–550
61 Rehman S, Tang T, Ali Z, Huang X, Hou Y. *Small*, 2017, 13: 1700087
62 Chen S, Wang L, Wu Q, Li X, Zhao Y, Lai H, Yang L, Sun T, Li Y, Wang X, Hu Z. *Sci China Chem*, 2015, 58: 180–186
63 Meng Y, Song W, Huang H, Ren Z, Chen SY, Suib SL. *J Am Chem Soc*, 2014, 136: 11452–11464
64 Giordano C, Antonietti M. *Nano Today*, 2011, 6: 366–380
65 Yang W, Rehman S, Chu X, Hou Y, Gao S. *ChemNanoMat*, 2015, 1: 376–398
66 Ham DJ, Lee JS. *Energies*, 2009, 2: 873–899
67 Mazza F, Trassatti S. *J Electrochem Soc*, 1963, 110: 847–849
68 Jing S, Luo L, Yin S, Huang F, Jia Y, Wei Y, Sun Z, Zhao Y. *Appl Catal B-Environ*, 2014, 147: 897–903
69 Dong Y, Li J. *Chem Commun*, 2015, 51: 572–575
70 An L, Huang W, Zhang N, Chen X, Xia D. *J Mater Chem A*, 2014, 2: 62–65
71 Qi J, Jiang L, Jiang Q, Wang S, Sun G. *J Phys Chem C*, 2010, 114: 18159–18166
72 Xia D, Liu S, Wang Z, Chen G, Zhang L, Zhang L, Hui SR, Zhang J. *J Power Sources*, 2008, 177: 296–302
73 Zhong H, Zhang H, Liang Y, Zhang J, Wang M, Wang X. *J Power Sources*, 2007, 164: 572–577
74 Zhang K, Zhang L, Chen X, He X, Wang X, Dong S, Han P, Zhang C, Wang S, Gu L, Cui G. *J Phys Chem C*, 2013, 117: 858–865
75 Tan S, Wang L, Saha S, Fushimi RR, Li D. *ACS Appl Mater Interfaces*, 2017, 9: 9815–9822
76 Yin S, Cai M, Wang C, Shen PK. *Energ Environ Sci*, 2011, 4: 558–563
77 Huang T, Yu J, Han J, Zhang Z, Xing Y, Wen C, Wu X, Zhang Y. *J Power Sources*, 2015, 300: 483–490
78 Deng D, Yu L, Chen X, Wang G, Jin L, Pan X, Deng J, Sun G, Bao X. *Angew Chem Int Ed*, 2013, 52: 371–375
79 Wen Z, Ci S, Zhang F, Feng X, Cui S, Mao S, Luo S, He Z, Chen J. *Adv Mater*, 2012, 24: 1399–1404
80 Jasinski R. *Nature*, 1964, 201: 1212–1213
81 Alt H, Binder H, Sandstede G. *J Catal*, 1973, 28: 8–19
82 Jahnke H, Schönborn M, Zimmermann G. Organic dyestuffs as catalysts for fuel cells. In: Schäfer FP, Gerischer H, Willig F, Meier H, Jahnke H, Schönborn M, Zimmermann G, Eds. *Physical and Chemical Applications of Dyestuffs*. Berlin Heidelberg: Springer, 1976.

133–181
83 Gupta S, Tryk D, Zecevic SK, Aldred W, Guo D, Savinell RF. *J Appl Electrochem*, 1998, 28: 673–682
84 Li X, Popov BN, Kawahara T, Yanagi H. *J Power Sources*, 2011, 196: 1717–1722
85 Koslowski UI, Abs-Wurmbach I, Fiechter S, Bogdanoff P. *J Phys Chem C*, 2008, 112: 15356–15366
86 Van Der Putten A, Elzing A, Visscher W, Barendrecht E. *J Electroanal Chem Interfacial Electrochem*, 1986, 205: 233–244
87 Yang W, Liu X, Yue X, Jia J, Guo S. *J Am Chem Soc*, 2015, 137: 1436–1439
88 Bae IT, Tryk DA, Scherson DA. *J Phys Chem B*, 1998, 102: 4114–4117
89 Niwa H, Horiba K, Harada Y, Oshima M, Ikeda T, Terakura K, Ozaki J, Miyata S. *J Power Sources*, 2009, 187: 93–97
90 Zhang Y, Huang LB, Jiang WJ, Zhang X, Chen YY, Wei Z, Wan LJ, Hu JS. *J Mater Chem A*, 2016, 4: 7781–7787
91 Jiang WJ, Gu L, Li L, Zhang Y, Zhang X, Zhang LJ, Wang JQ, Hu JS, Wei Z, Wan LJ. *J Am Chem Soc*, 2016, 138: 3570–3578
92 Chung HT, Cullen DA, Higgins D, Sneed BT, Holby EF, More KL, Zelenay P. *Science*, 2017, 357: 479–484
93 Osmieri L, Monteverde Videla AHA, Armandi M, Specchia S. *Int J Hydrogen Energ*, 2016, 41: 22570–22588
94 Wu G, Santandreu A, Kellogg W, Gupta S, Ogoke O, Zhang H, Wang HL, Dai L. *Nano Energ*, 2016, 29: 83–110
95 Shao M, Chang Q, Dodelet JP, Chenitz R. *Chem Rev*, 2016, 116: 3594–3657
96 Gong K, Du F, Xia Z, Durstock M, Dai L. *Science*, 2009, 323: 760–764
97 Zhang C, Mahmood N, Yin H, Liu F, Hou Y. *Adv Mater*, 2013, 25: 4932–4937
98 Yang S, Zhi L, Tang K, Feng X, Maier J, Müllen K. *Adv Funct Mater*, 2012, 22: 3634–3640
99 Fazio G, Ferrighi L, Di Valentin C. *J Catal*, 2014, 318: 203–210
100 Zhang C, Hao R, Liao H, Hou Y. *Nano Energ*, 2013, 2: 88–97
101 Lai L, Potts JR, Zhan D, Wang L, Poh CK, Tang C, Gong H, Shen Z, Lin J, Ruoff RS. *Energ Environ Sci*, 2012, 5: 7936
102 Chen P, Xiao TY, Qian YH, Li SS, Yu SH. *Adv Mater*, 2013, 25: 3192–3196
103 Hu W, Wang Q, Wu S, Huang Y. *J Mater Chem A*, 2016, 4: 16920–16927
104 Zhang C, Fu L, Liu N, Liu M, Wang Y, Liu Z. *Adv Mater*, 2011, 23: 1020–1024
105 Zhang L, Su Z, Jiang F, Yang L, Qian J, Zhou Y, Li W, Hong M. *Nanoscale*, 2014, 6: 6590–6602
106 Zheng Y, Jiao Y, Ge L, Jaroniec M, Qiao SZ. *Angew Chem*, 2013, 125: 3192−3198
107 Zhang J, Qu L, Shi G, Liu J, Chen J, Dai L. *Angew Chem*, 2016, 128: 2270–2274